NASA Contractor Report 204143
ICOMP–97–10; CMOTT–97–05

CMOTT Turbulence Module for NPARC

J. Zhu and T.-H. Shih
Institute for Computational Mechanics in Propulsion and
Center for Modeling of Turbulence and Transition
Cleveland, Ohio

August 1997

Prepared for
Lewis Research Center
Under Cooperative Agreement NCC3–520

National Aeronautics and
Space Administration

CMOTT Turbulence Module for NPARC

J. Zhu and T.-H. Shih
Center for Modeling of Turbulence and Transition
ICOMP, OAI, NASA Lewis Research Center
Cleveland, Ohio 44135

Summary

This is a user's manual of the CMOTT turbulence module, version 2.0, developed for the NPARC code. The module is written in a self-contained manner so that the user can use any turbulence model in the module without concern as to how it is implemented and solved. Three two-equation turbulence models have been built into the module: Chien, Shih-Lumley and CMOTT models, and all of them have both the low Reynolds number and wall function options. Unlike Chien's model, both the Shih-Lumley and CMOTT models do not involve the dimensionless wall distance y^+ in the low Reynolds number approach, an advantage for separated flow calculations. The Van Driest transformation is used so that the wall functions can be applied to both incompressible and compressible flows. The manual gives the details of the turbulence models used and their numerical implementation. It also gives two application examples, one for subsonic and the other for transonic flow, for demonstration. The module can be easily linked to the NPARC code for practical applications.

Contents

1 Introduction

This manual describes the version 2.0 of the CMOTT turbulence module developed at the Center for Modeling Of Turbulence and Transition (CMOTT) for the NPARC code (Cooper and Sirbaugh, 1989 and 1990). The present version differs from the previous one (Zhu and Shih, 1995) in the following two major aspects: 1) use of the delta form of turbulence transport equations, and 2) inclusion of the wall function approach.

The purpose of developing the turbulence module is to enhance the turbulence modeling capability of NPARC. The module is written in such a way that it, on the one hand, can be easily linked to NPARC for practical calculations, and on the other hand, can be updated in time to include the state of the art of turbulence models suitable for applications in aerospace and aero-propulsion systems. With the aid of the module, turbulence model developers can also take the advantage of the well-established and sophisticated CFD code to test turbulence models under development for a variety of complex flows which are intractable with simple research codes.

Under the widely used Boussinesq's isotropic eddy-viscosity concept, the Reynolds-averaged equations governing turbulent flows are of the same form as those governing laminar flows, except that the laminar viscosity μ is replaced by the effective viscosity

$$\mu_{eff} = \mu + \mu_t \tag{1}$$

Therefore, a mean flow solver can be used to calculate turbulent flows once the turbulent eddy-viscosity μ_t is available. For most CFD codes, especially those for compressible flow calculations, the laminar viscosity μ is a variable not a constant. In this case, few changes are required for a mean flow solver to use the turbulence module. The input to the module are the mean flow variables, boundary and geometric information which are to be provided by a mean flow solver. The output of the module are the turbulent eddy-viscosity μ_t and relevant turbulent source terms which are needed for the mean flow calculation. The interaction between the mean flow solver and the turbulence module will give the final turbulent flow solution.

In the module, the three low Reynolds number K-ϵ turbulence models have been implemented: Chien (1982), Shih-Lumley (1993) and CMOTT realizable models (Yang et al., 1995; Zhu and Shih, 1995). Chien's model is one of the well-known low Reynolds number K-ϵ models. However, it has some undesirable deficiencies. First, a near wall pseudo-dissipation rate is introduced to remove the singularity in the dissipation rate equation at the wall. The definition of the near wall pseudo-dissipation rate is quite arbitrary. Second, the model constants are different from those of the standard K-ϵ model (Launder and Spalding, 1974), making the near wall model less capable of handling flows containing both high Reynolds number turbulence and near wall turbulence. Patel et al. (1985) required as the first criterion, the ability of the near wall models to be able to predict turbulent free shear flows. Third, the dimensionless wall distance y^+ is used in the damping function f_μ for the eddy-viscosity. Because the y^+ involves the friction velocity U_τ which is equal to zero at separation or reattachment points, any model using

y^+ may have difficulties for separated flows. The Shih-Lumley and CMOTT models are free of these deficiencies. The two models differ from one another in the C_μ formulation, one using the standard constant and the other a new formulation. The new C_μ has the following desirable features: (a) It is derived from a rigorous realizability analysis (Shih et al., 1994) that requires the non-negativity of the turbulent normal stresses and Schwarz' inequality between any fluctuating quantities. As a result, unlike most of the existing models, it satisfies the realizability conditions. (b) It accounts for the effect of the mean deformation rate by which the eddy-viscosity will be significantly reduced to an adequate level to mimic complex flow structures. (c) It is easier to use, as compared with other formulations. Simplicity is of great value for practical engineering applications. Successful applications of this new C_μ formulation can be found in Shih et al. (1994 and 1995). The module with these turbulence models has been applied to a number of flows including flows over a flat plate, in an ejector nozzle, in a transonic diffuser, and a boat-tail nozzle flow (Yang et al., 1995). For all the flow cases tested so far, it has been found that both the Shih-Lumley and CMOTT models produce improved or similar predictions compared with the Chien model. The CMOTT model with variable C_μ turns out to be more computationally robust than the other two. It was able to give numerical solutions in cases where the models with constant C_μ suffered from numerical instability.

The major problems or difficulties associated with the low Reynolds number turbulence models are: 1) They require very fine grid spacing in near-wall regions, thus increasing considerably computational burden, especially in three-dimensional cases. Moreover, the highly stretched nature of mesh distribution may have an adverse impact on numerical stability. 2) Most of models are not of tensorial invariant form, that is, they contain a distance parameter normal to the wall. The wall-distance dependency causes inconvenience for model applications in complicated geometries. Currently, great effort is being given in the area of near-wall turbulence modeling to remove this dependency, but no satisfactory result has been obtained yet. 3) Most of the low Reynolds number turbulence models were fine-tuned against attached flows, which is, of course, not sufficient to guarantee their good performance for separated flows.

An alternative is to use the high Reynolds number turbulence models. Here, the governing equations are integrated to a point far outside the viscous sublayer rather than down to the wall, and the near-wall region is bridged over with the wall functions. Although in theory the wall function approach is only valid for certain attached flows with no pressure gradient and mass transfer, it has been applied in practice to many separated flows with varing degree of success. For those flows where maximum shear stresses occur far away from the wall, the near-wall turbulence modeling is not critical for overall flow simulations. In these cases, use of the wall functions has a very beneficial effect on the stability and economy of computations. Although the principle argument for originally adopting the wall function approach (economy of grid points) has been weakened as larger and faster computers have become available, it will still find its applications in predicting complex flows, especially for large scale engineering problems.

In the present work, we extend the turbulence module by including the wall functions.

For incompressible flows, the universal law of the wall may be expressed as

$$\frac{U}{U_\tau} = \frac{1}{\kappa} \ln\left(\frac{\rho U_\tau y}{\mu}\right) + C \tag{2}$$

where $\kappa = 0.41$ and $C = 5.2$. The derivation of Eq. (2) is based on the assumption that the shear stress in the region close to the wall is constant and equal to the wall shear stress. It has been shown (Viegas et al., 1985; Huang and Coakley, 1993) that the same form also exists for compressible flows with the velocity U being replaced by the Van Driest transformed velocity U_c (Van Driest, 1951). For the K-ϵ turbulence models, the convection and diffusion terms of their transport equations are negligible in the inertial sublayer so that local equilibrium prevails, which implies that the production of the turbulent kinetic energy K is equal to the dissipation rate ϵ of K. The local equilibrium condition leads to two simple relations which can be used as boundary conditions for K and ϵ for both incompressible and compressible flows.

Although the wall functions look simple, their numerical implementation is not trivial. The main difficulty comes from the logarithmic law in which both U and U_τ are unknown, and U_τ cannot explicitly be solved for. It is prone to being numerically unstable if one uses Eq. (2) and iteratively solves U_τ to obtain the boundary conditions for the Navier-Stokes equations. In the module, we use an implicit procedure which directly incorporates Eq. (2) into the Navier Stokes equations. In this way, there is no need to solve Eq. (2) for U_τ by sub-iteration. The implicit method turns out to be more stable than the explicit one. Another important issue is the artificial viscosity. Chitsomboon (1994) found that the artificial viscosity originally implemented in the NPARC code totally spoiled the solution of the wall functions. This was because the artificial viscosity became unrealistically large in the vicinity of walls due to very steep velocity gradients resulting from the coarseness of grid spacing as required by the wall function approach. He fixed up this problem by extrapolating velocities at the wall rather than using the physical values of no-slip velocities, when calculating the artificial viscosity. In the module, we simply turn off the artificial viscosity in the near-wall region.

In general, turbulence model equations require special treatment to ensure numerical realizability such as the positiveness of K and ϵ. They are also often of source-dominate nature, which sometimes makes the linearization of source terms crucial for computational stability. Due to these considerations, we used the non-delta form of the transport equations in the previous version of the module (Zhu and Shih, 1995). The non-delta form leads to simpler linearization and is more effective to ensure the positiveness of the turbulent kinetic energy and its dissipation rate than the delta form. However, the non-delta formulation requires 8 additional arrays in the three-dimensional code, and the above advantages did not manifest themselves to be obvious in all the test cases computed so far, which may be due to the fact that, on the one hand, the stability of solution process is constrained largely by the mean flow solver, and on the other hand, positivity for models of K-ϵ type can be ensured by simple numerical measure such as clipping. Therefore, the present module uses the delta form, which is in line with the NPARC code.

2 Turbulence Models

2.1 General Form

In accordance with the NPARC code, a non-dimensional form of equations is adopted. The three low Reynolds number two-equation turbulence models built into the module have the following common form in which the Reynolds stresses $\tau_{ij}(= -\rho\overline{u_i u_j})$ are calculated by

$$\tau_{ij} = R_e^{-1}\mu_t(U_{i,j} + U_{j,i} - \frac{2}{3}U_{k,k}) - \frac{2}{3}\rho K\delta_{ij} \tag{3}$$

where R_e is the reference Reynolds number. The turbulent eddy viscosity μ_t, the turbulent kinetic energy K and its dissipation rate ϵ are calculated by the following equations

$$\mu_t = R_e f_\mu C_\mu \rho K^2/\epsilon \tag{4}$$

$$(\rho K)_{,t} + [\rho U_j K - R_e^{-1}(\mu + \frac{\mu_t}{\sigma_K})K_{,j}]_{,j} = P - \rho\epsilon + D \tag{5}$$

$$(\rho\epsilon)_{,t} + [\rho U_j \epsilon - R_e^{-1}(\mu + \frac{\mu_t}{\sigma_\epsilon})\epsilon_{,j}]_{,j} = f_1 C_1 \frac{\epsilon}{K}P - f_2 C_2 \rho\frac{\epsilon^2}{K} + E \tag{6}$$

where

$$P = \tau_{ij}U_{i,j} \tag{7}$$

$$f_1 = 1, \qquad f_2 = 1 - 0.22\exp[-(R_t/6)^2], \quad R_t = \frac{R_e\rho K^2}{\mu\epsilon} \tag{8}$$

P is the turbulent production. For high Reynolds number models, $f_\mu = f_1 = f_2 = 1$ and $D = E = 0$. The differences in the three models are given below.

2.2 Low Reynolds Number Form

Chien's K-ϵ model.

$$C_\mu = 0.09,\ C_1 = 1.35,\ C_2 = 1.8,\ \sigma_K = 1,\ \sigma_\epsilon = 1.3 \tag{9}$$

$$f_\mu = 1 - \exp(-0.0115y^+), \qquad y^+ = \frac{R_e\rho u_\tau y_n}{\mu} \tag{10}$$

$$D = -2R_e^{-1}\mu\frac{K}{y_n^2} \tag{11}$$

$$E = -\frac{2R_e^{-1}\mu\epsilon}{y_n^2}\exp(-0.5y^+) \tag{12}$$

At the wall, the values of K and ϵ are both set to zero.

Shih-Lumley's K-ϵ model.

$$C_\mu = 0.09,\ C_1 = 1.44,\ C_2 = 1.92,\ \sigma_K = 1,\ \sigma_\epsilon = 1.3 \tag{13}$$

$$f_\mu = [1 - \exp(-a_1 R_k - a_3 R_k^3 - a_5 R_k^5)]^{1/2}, \quad R_K = \frac{R_e \rho K^{1/2} y_n}{\mu} \tag{14}$$

$$a_1 = 1.7 * 10^{-3},\ a_3 = 10^{-9},\ a_5 = 5 * 10^{-10}$$

$$D = 0 \tag{15}$$

$$E = \frac{\mu \mu_t}{\rho R_e^2} S_{,i} S_{,i} \tag{16}$$

$$S = \sqrt{2 S_{ij}^* S_{ji}^*}, \quad S_{ij}^* = \frac{1}{2}(U_{i,j} + U_{j,i}) - \frac{1}{3} U_{k,k} \delta_{ij} \tag{17}$$

The wall boundary conditions for K and ϵ are

$$K = 0.250 u_\tau^2, \quad \epsilon = 0.251 R_e \frac{\rho u_\tau^4}{\mu} \tag{18}$$

CMOTT K-ϵ model. This model is the same as the Shih-Lumley model, except that C_μ is calculated by

$$C_\mu = \min[0.09,\ (A_0 + A_s U^* K/\epsilon)^{-1}] \tag{19}$$

where

$$A_0 = 4, \quad A_s = \sqrt{6} \cos\phi \tag{20}$$

$$U^* = \sqrt{S_{ij}^* S_{ij}^* + \Omega_{ij} \Omega_{ij}} \tag{21}$$

$$\phi = \frac{1}{3} arc\cos(\sqrt{6} W), \quad W = \frac{S_{ij}^* S_{jk}^* S_{ki}^*}{(S^*)^3} \tag{22}$$

$$S^* = \sqrt{S_{ij}^* S_{ij}^*}, \quad \Omega_{ij} = \frac{1}{2}(U_{i,j} - U_{j,i}) \tag{23}$$

In the above formulas, y_n refers to the normal distance from the wall.

2.3 Wall Functions

The compressible law of the wall (Huang and Coakley, 1993) is used in the turbulence module. Following the NPARC nondimensionalization, this law can be written as

$$U_c^+ = \frac{U_c}{U_\tau} = \frac{1}{\kappa}\ln(Ey^+) \tag{24}$$

where

$$\begin{aligned} U_\tau &= \sqrt{(\tau/\rho)_{wall}} \\ y^+ &= R_e U_\tau y(\rho/\mu)_{wall} \\ \kappa &= 0.41, \quad E = 8.4317 \end{aligned} \tag{25}$$

and U_c is the Van Driest transformed velocity defined by (Van Driest, 1951):

$$U_c = \sqrt{B}\left[\sin^{-1}\left(\frac{A+U}{D}\right) - \sin^{-1}\left(\frac{A}{D}\right)\right] \tag{26}$$

where

$$\begin{aligned} A &= \left(\frac{q}{\tau}\right)_{wall} \\ B &= \frac{2T_{wall}}{(\gamma-1)P_{rt}} \\ D &= \sqrt{A^2+B} \end{aligned} \tag{27}$$

In the near-wall region, with the convection neglected the energy equation can be reduced to give an expression for the total heat flux

$$q = q_{wall} + U\tau \tag{28}$$

and with the local equilibrium assumption (Launder and Spalding, 1974), the turbulent kinetic energy K and its dissipation rate ϵ can be calculated by

$$K = \frac{\tau_{wall}/\rho}{0.3} \tag{29}$$

$$\epsilon = \frac{(\tau_{wall}/\rho)^{3/2}}{\kappa y} \tag{30}$$

In the above expressions, the subscript *wall* refers to the value of the corresponding function at the wall. Equations (24) and (28) - (30) form the wall functions which are used to bridge over the first grid point and the solid wall.

3 Calculation Procedure

The following presentation is only restricted to the numerical aspects related to the turbulence module. Refer to Cooper and Sirbaugh (1989 and 1990) about the details of the NPARC code.

3.1 General Form of Turbulence Equations

The turbulent transport equations (5) and (6) in general curvilinear coordinates (ξ, η, ζ) may be written in the following form:

$$\partial_t Q + \partial_\xi F_1 + \partial_\eta F_2 + \partial_\zeta F_3 = \partial_\xi G_1 + \partial_\eta G_2 + \partial_\zeta G_3 + S \tag{31}$$

where

$$Q = J^{-1}\begin{bmatrix} \rho K \\ \rho\epsilon \end{bmatrix}, \quad F_i = J^{-1}\begin{bmatrix} \rho U_i K \\ \rho U_i \epsilon \end{bmatrix}, \quad G_i = J^{-1}\begin{bmatrix} \mu_K \nabla\xi_i \cdot \nabla K \\ \mu_\epsilon \nabla\xi_i \cdot \nabla\epsilon \end{bmatrix} \tag{32}$$

$$U_1 = U, \quad U_2 = V, \quad U_3 = W \tag{33}$$

$$\xi_1 = \xi, \quad \xi_2 = \eta, \quad \xi_3 = \zeta \tag{34}$$

$$\mu_K = R_e^{-1}(\mu + \frac{\mu_t}{\sigma_K}) \tag{35}$$

$$\mu_\epsilon = R_e^{-1}(\mu + \frac{\mu_t}{\sigma_\epsilon}) \tag{36}$$

$$\begin{aligned} \nabla\xi \cdot \nabla\phi &= (\xi_x^2 + \xi_y^2 + \xi_z^2)\partial_\xi\phi \\ &+ (\xi_x\eta_x + \xi_y\eta_y + \xi_z\eta_z)\partial_\eta\phi + (\xi_x\zeta_x + \xi_y\zeta_y + \xi_z\zeta_z)\partial_\zeta\phi \end{aligned} \tag{37}$$

$$\begin{aligned} \nabla\eta \cdot \nabla\phi &= (\eta_x^2 + \eta_y^2 + \eta_z^2)\partial_\eta\phi \\ &+ (\eta_x\xi_x + \eta_y\xi_y + \eta_z\xi_z)\partial_\xi\phi + (\eta_x\zeta_x + \eta_y\zeta_y + \eta_z\zeta_z)\partial_\zeta\phi \end{aligned} \tag{38}$$

$$\begin{aligned} \nabla\zeta \cdot \nabla\phi &= (\zeta_x^2 + \zeta_y^2 + \zeta_z^2)\partial_\zeta\phi \\ &+ (\zeta_x\xi_x + \zeta_y\xi_y + \zeta_z\xi_z)\partial_\xi\phi + (\zeta_x\eta_x + \zeta_y\eta_y + \zeta_z\eta_z)\partial_\eta\phi \end{aligned} \tag{39}$$

J is Jacobian of coordinate transformation, U, V and W are the contravarient velocities, $\phi = K$ or ϵ, and S contains the source terms in Eqs.(5) and (6), respectively.

3.2 Time Differencing

By using Euler backward differencing, Eq.(31) can be written as

$$\Delta Q + \Delta t[\partial_\xi F_1^{n+1} + \partial_\eta F_2^{n+1} + \partial_\zeta F_3^{n+1} - (\partial_\xi G_1^{n+1} + \partial_\eta G_2^{n+1} + \partial_\zeta G_3^{n+1} + S^{n+1})] = 0 \quad (40)$$

where

$$\Delta Q = Q^{n+1} - Q^n \quad (41)$$

$$\Delta t = t^{n+1} - t^n \quad (42)$$

and the superscript n refers to the time level.

3.3 Time Linearization

Eq.(40) can be linearized by expressing all flux vectors in terms of the conservation variable vector Q

$$F_i^{n+1} = F_i^n + \Delta t \partial_t F_i = F_i^n + A_i \Delta Q \quad (43)$$

$$G_i^{n+1} = G_i^n + \Delta t \partial_t G_i = G_i^n + B_i \Delta Q \quad (44)$$

$$S^{n+1} = S^n + \Delta t \partial_t S = S^n + C \Delta Q \quad (45)$$

where

$$A_i = \frac{\partial F_i}{\partial Q} = \begin{bmatrix} U_i & 0 \\ 0 & U_i \end{bmatrix} \quad (46)$$

$$B_i = \frac{\partial G_i}{\partial Q} = \begin{bmatrix} b_{11}^i & 0 \\ 0 & b_{22}^i \end{bmatrix} \quad (47)$$

$$C = \frac{\partial S}{\partial Q} = \begin{bmatrix} c_{11} & c_{12} \\ c_{21} & c_{22} \end{bmatrix} \quad (48)$$

$$
\begin{aligned}
b_{11}^1 &= [\alpha^1\partial_\xi + J^{-1}\mu_K(\xi_x\eta_x + \xi_y\eta_y + \xi_z\eta_z)\partial_\eta + J^{-1}\mu_K(\xi_x\zeta_x + \xi_y\zeta_y + \xi_z\zeta_z)\partial_\zeta](J/\rho) \\
b_{22}^1 &= [\beta^1\partial_\xi + J^{-1}\mu_\epsilon(\xi_x\eta_x + \xi_y\eta_y + \xi_z\eta_z)\partial_\eta + J^{-1}\mu_\epsilon(\xi_x\zeta_x + \xi_y\zeta_y + \xi_z\zeta_z)\partial_\zeta](J/\rho) \\
b_{11}^2 &= [\alpha^2\partial_\eta + J^{-1}\mu_K(\eta_x\xi_x + \eta_y\xi_y + \eta_z\xi_z)\partial_\xi + J^{-1}\mu_K(\eta_x\zeta_x + \eta_y\zeta_y + \eta_z\zeta_z)\partial_\zeta](J/\rho) \\
b_{22}^2 &= [\beta^2\partial_\eta + J^{-1}\mu_\epsilon(\eta_x\xi_x + \eta_y\xi_y + \eta_z\xi_z)\partial_\xi + J^{-1}\mu_\epsilon(\eta_x\zeta_x + \eta_y\zeta_y + \eta_z\zeta_z)\partial_\zeta](J/\rho) \\
b_{11}^3 &= [\alpha^3\partial_\zeta + J^{-1}\mu_K(\zeta_x\xi_x + \zeta_y\xi_y + \zeta_z\xi_z)\partial_\xi + J^{-1}\mu_k(\zeta_x\eta_x + \zeta_y\eta_y + \zeta_z\eta_z)\partial_\eta](J/\rho) \\
b_{22}^3 &= [\beta^3\partial_\zeta + J^{-1}\mu_\epsilon(\zeta_x\xi_x + \zeta_y\xi_y + \zeta_z\xi_z)\partial_\xi + J^{-1}\mu_\epsilon(\zeta_x\eta_x + \zeta_y\eta_y + \zeta_z\eta_z)\partial_\eta](J/\rho)
\end{aligned}
\tag{49}
$$

$$
\begin{aligned}
\alpha^1 &= J^{-1}\mu_K(\xi_x^2 + \xi_y^2 + \xi_z^2), & \beta^1 &= J^{-1}\mu_\epsilon(\xi_x^2 + \xi_y^2 + \xi_z^2) \\
\alpha^2 &= J^{-1}\mu_K(\eta_x^2 + \eta_y^2 + \eta_z^2), & \beta^2 &= J^{-1}\mu_\epsilon(\eta_x^2 + \eta_y^2 + \eta_z^2) \\
\alpha^3 &= J^{-1}\mu_K(\zeta_x^2 + \zeta_y^2 + \zeta_z^2), & \beta^3 &= J^{-1}\mu_\epsilon(\zeta_x^2 + \zeta_y^2 + \zeta_z^2)
\end{aligned}
\tag{50}
$$

After introducing Eqs.(43)-(45), Eq.(40) becomes

$$
\{I + \Delta t[\partial_\xi A_1 + \partial_\eta A_2 + \partial_\zeta A_3 - (\partial_\xi B_1 + \partial_\eta B_2 + \partial_\zeta B_3 + C)]\}\Delta Q = RHS \tag{51}
$$

where

$$
RHS = \Delta t(-\partial_\xi F_1^n - \partial_\eta F_2^n - \partial_\zeta F_3^n + \partial_\xi G_1^n + \partial_\eta G_2^n + \partial_\zeta G_3^n + S^n) \tag{52}
$$

I is an identity matrix.

3.4 Approximate Factorization

By using the approximate factorization method, the three-dimensional equation (51) can be reduced to the following three unidimensional equations

$$
[I + \Delta t(\partial_\xi A_1 - \partial_\xi B_1)]\Delta Q^{**} = RHS \tag{53}
$$

$$
[I + \Delta t(\partial_\eta A_2 - \partial_\eta B_2)]\Delta Q^{*} = \Delta Q^{**} \tag{54}
$$

$$
[I + \Delta t(\partial_\zeta A_3 - \partial_\zeta B_3 - C)]\Delta Q = \Delta Q^{*} \tag{55}
$$

Solving sequentially these equations finally gives the solution of Eq.(31)

$$
Q^{n+1} = Q^n + \Delta Q \tag{56}
$$

3.5 Space Differencing (LHS)

For steady-state computations, differencing the left-hand side (LHS) of Eqs.(53)-(55) is not crucial to the accuracy of final solutions. Therefore, the first-order accurate upwinding is used for the inviscid flux terms and the central-differencing is used for all the other terms.

With the first-order upwinding, the inviscid terms in Eq.(53) can be written as

$$A_1 = A_1^+ + A_1^-, \qquad A_1^+ = \begin{bmatrix} U^+ & 0 \\ 0 & U^+ \end{bmatrix}, \qquad A_1^- = \begin{bmatrix} U^- & 0 \\ 0 & U^- \end{bmatrix} \tag{57}$$

$$U^+ = 0.5(U + |U|), \qquad U^- = 0.5(U - |U|) \tag{58}$$

$$\begin{aligned} \partial_\xi U \Delta q^1 &= U_j^+ \Delta q_j^1 - U_{j-1}^+ \Delta q_{j-1}^1 + U_{j+1}^- \Delta q_{j+1}^1 - U_j^- \Delta q_j^1 \\ \partial_\xi U \Delta q^2 &= U_j^+ \Delta q_j^2 - U_{j-1}^+ \Delta q_{j-1}^2 + U_{j+1}^- \Delta q_{j+1}^2 - U_j^- \Delta q_j^2 \end{aligned} \tag{59}$$

where Δq^1 and Δq^2 are the components of the intermediate vector ΔQ^{**}.

By using the central-differencing and neglecting cross-derivative terms in Eq.(49), the viscous terms in Eq.(53) can be written

$$\begin{aligned} \partial_\xi b_{11}^1 \Delta q^1 = \; & 0.5\{(\alpha_{j+1}^1 + \alpha_j^1)[(J/\rho)_{j+1}\Delta q_{j+1}^1 - (J/\rho)_j \Delta q_j^1] \\ & -(\alpha_j^1 + \alpha_{j-1}^1)[(J/\rho)_j \Delta q_j^1 - (J/\rho)_{j-1}\Delta q_{j-1}^1]\} \\ \partial_\xi b_{22}^1 \Delta q^2 = \; & 0.5\{(\beta_{j+1}^1 + \beta_j^1)[(J/\rho)_{j+1}\Delta q_{j+1}^2 - (J/\rho)_j \Delta q_j^2] \\ & -(\beta_j^1 + \beta_{j-1}^1)[(J/\rho)_j \Delta q_j^2 - (J/\rho)_{j-1}\Delta q_{j-1}^2]\} \end{aligned} \tag{60}$$

After introducing Eqs.(59) and (60) into Eq.(53), we have

$$\begin{aligned} A_j^{11}\Delta q_{j-1}^1 + B_j^{11}\Delta q_j^1 + C_j^{11}\Delta q_{j+1}^1 &= r^1 \\ A_j^{22}\Delta q_{j-1}^2 + B_j^{22}\Delta q_j^2 + C_j^{22}\Delta q_{j+1}^2 &= r^2 \end{aligned} \tag{61}$$

where

$$\begin{aligned} A_j^{11} &= -\Delta t[U_{j-1}^+ + 0.5(\alpha_{j-1}^1 + \alpha_j^1)(J/\rho)_{j-1}] \\ B_j^{11} &= 1 + \Delta t[U_j^+ - U_j^- + 0.5(\alpha_{j+1}^1 + 2\alpha_j^1 + \alpha_{j-1}^1)(J/\rho)_j] \\ C_j^{11} &= \Delta t[U_{j+1}^- - 0.5(\alpha_{j+1}^1 + \alpha_j^1)(J/\rho)_{j+1}] \end{aligned} \tag{62}$$

$$
\begin{aligned}
A_j^{22} &= -\Delta t[U_{j-1}^{+} + 0.5(\beta_{j-1}^{1} + \beta_j^{1})(J/\rho)_{j-1}] \\
B_j^{22} &= 1 + \Delta t[U_j^{+} - U_j^{-} + 0.5(\beta_{j+1}^{1} + 2\beta_j^{1} + \beta_{j-1}^{1})(J/\rho)_j] \\
C_j^{22} &= \Delta t[U_{j+1}^{-} - 0.5(\beta_{j+1}^{1} + \beta_j^{1})(J/\rho)_{j+1}]
\end{aligned} \tag{63}
$$

and r^1 and r^2 are the components of the vector RHS.

The same procedure can be used for Eqs.(54) and (55), except that for Eq.(55), the coefficients B in Eqs. (62) and (63) are replaced by

$$
\begin{aligned}
B_l^{11} &= B_l^{11} - c_{11}\Delta t \\
B_l^{12} &= B_l^{12} - c_{12}\Delta t \\
B_l^{21} &= B_l^{21} - c_{21}\Delta t \\
B_l^{22} &= B_l^{22} - c_{22}\Delta t
\end{aligned} \tag{64}
$$

3.6 Space Differencing (RHS)

To ensure both accuracy and stability of numerical solutions, the hybrid linear/parabolic approximation (HLPA) scheme (Zhu, 1991) is used to calculate the convection terms of the right-hand side (RHS) in Eq.(52). It has been shown (Zhu, 1992) that the HLPA scheme of second-order accuracy works nearly as well as the third-order accurate SMART (Gaskell and Lau,1988) and SHARP (Leonard,1988) schemes in terms of eliminating numerical diffusion while retaining boundedness of numerical solutions. Consider the inviscid flux in the ξ direction. The HLPA scheme evaluates the value of variable ϕ at the cell-face $j-1/2$ as follows

$$
\phi_{j-1/2} = U_{j-1/2}^{+}\phi_{j-1} + U_{j-1/2}^{-}\phi_j + \delta\phi \tag{65}
$$

where

$$
\delta\phi = U_{j-1/2}^{+}\alpha_{j-1/2}^{+}(\phi_j - \phi_{j-1})\frac{\phi_{j-1} - \phi_{j-2}}{\phi_j - \phi_{j-2}} + U_{j-1/2}^{-}\alpha_{j-1/2}^{-}(\phi_{j-1} - \phi_j)\frac{\phi_j - \phi_{j+1}}{\phi_{j-1} - \phi_{j+1}} \tag{66}
$$

$$
\begin{aligned}
\alpha_{j-1/2}^{+} &= \begin{cases} 1 & \text{if } |(\phi_j - 2\phi_{j-1} + \phi_{j-2})/(\phi_j - \phi_{j-2})| < 1 \\ 0 & \text{otherwise} \end{cases} \\
\alpha_{j-1/2}^{-} &= \begin{cases} 1 & \text{if } |(\phi_{j-1} - 2\phi_j + \phi_{j+1})/(\phi_{j-1} - \phi_{j+1})| < 1 \\ 0 & \text{otherwise} \end{cases}
\end{aligned} \tag{67}
$$

and U^+ and U^- are defined in Eq.(58).

It can be seen that Eq.(65) is in fact the result of the first-order accurate upwinding with an additional term $\delta\phi$ added. The additional term may be viewed as an antidiffusive correction to the upwinding. The conventional central differencing scheme is used to calculate all the other terms in RHS.

3.7 Source Terms

For the source term in Eq.(31), we have

$$S = \begin{bmatrix} S_1 \\ S_2 \end{bmatrix}, \qquad \begin{aligned} S_1 &= J^{-1}[P - \rho\epsilon + D] \\ S_2 &= J^{-1}[(C_1 P - f_2 C_2 \rho\epsilon)\epsilon/K + E] \end{aligned} \tag{68}$$

and the elements in the source term Jacobian matrix C in Eq.(48) are calculated by

$$c_{11} = \frac{\partial S_1}{\partial Q_1}, \quad c_{12} = \frac{\partial S_1}{\partial Q_2}, \quad c_{21} = \frac{\partial S_2}{\partial Q_1}, \quad c_{22} = \frac{\partial S_2}{\partial Q_2} \tag{69}$$

where

$$Q_1 = J^{-1}\rho K, \qquad Q_2 = J^{-1}\rho\epsilon \tag{70}$$

From the stability requirement for the type of Eq.(61), we have

$$c_{11}\ ,\ c_{12}\ ,\ c_{21}\ ,\ c_{22}\ \leq 0 \tag{71}$$

Noting that certain degree of freedom exists in dealing with the left-hand side terms of Eq.(51) for steady-state calculations, we tested the following two linearization methods:

Method 1. By "exactly" calculating the derivatives in Eq.(69), we obtain

$$\begin{cases} c_{11} = 2\dfrac{P}{\rho K} + \dfrac{\partial(J^{-1}D)}{\partial Q_1} \\ c_{12} = -\dfrac{P}{\rho\epsilon} - 1 + \dfrac{\partial(J^{-1}D)}{\partial Q_2} \\ c_{21} = C_1 P\dfrac{\epsilon}{\rho K^2} + C_2\dfrac{\epsilon^2}{K^2}[f_2 + \dfrac{4R_t^2}{36}(f_2 - 1)] + \dfrac{\partial(J^{-1}E)}{\partial Q_1} \\ c_{22} = -2C_2\dfrac{\epsilon}{K}[f_2 + \dfrac{R_t^2}{36}(f_2 - 1)] + \dfrac{\partial(J^{-1}E)}{\partial Q_2} \end{cases} \tag{72}$$

which do not satisfy the stability requirement Eq.(71).

Method 2. Neglecting the D and E terms, we can write the source term as

$$\begin{aligned} S_1 &= J^{-1}P - \frac{\epsilon}{K}Q_1 \\ S_2 &= J^{-1}C_1 P\frac{\epsilon}{K} - \frac{f_2 C_2 \epsilon}{K}Q_2 \end{aligned} \tag{73}$$

and the derivatives can be formally written as

$$\begin{cases} c_{11} = -\dfrac{\epsilon}{K} \\ c_{12} = 0 \\ c_{21} = 0 \\ c_{22} = -\dfrac{f_2 C_2 \epsilon}{K} \end{cases} \tag{74}$$

which meet the stability requirement Eq.(71).

Numerical tests conducted so far have shown that both methods produce little difference in terms of both convergence rate and accuracy. Therefore, only the method 2 which leads to a rather simple implementation is adopted in the present module.

3.8 Wall Function Implementation

In the NPARC code, the following nondimensional, Reynolds-averaged Navier-Stokes equations are solved:

$$\frac{\partial \hat{Q}}{\partial t} + \frac{\partial \hat{F}_1}{\partial \xi} + \frac{\partial \hat{F}_2}{\partial \eta} + \frac{\partial \hat{F}_3}{\partial \zeta} = \frac{\partial \hat{G}_1}{\partial \xi} + \frac{\partial \hat{G}_2}{\partial \eta} + \frac{\partial \hat{G}_3}{\partial \zeta} \tag{75}$$

where $\hat{Q}$, $\hat{F}_j$ and $\hat{G}_j$ $(j = 1,2,3)$ are the conservation variable vector, inviscid flux vectors and viscous flux vectors, respectively. Because only the viscous flux vectors need to be modified with the use of the wall functions, their detailed forms are given below:

$$\hat{G}_1 = \begin{bmatrix} g_{11} \\ g_{12} \\ g_{13} \\ g_{14} \\ g_{15} \end{bmatrix}, \qquad \begin{aligned} g_{11} &= 0 \\ g_{12} &= \hat{\tau}_{11} = J^{-1}(\xi_x \tau_{11} + \xi_y \tau_{12} + \xi_z \tau_{13}) \\ g_{13} &= \hat{\tau}_{12} = J^{-1}(\xi_x \tau_{21} + \xi_y \tau_{22} + \xi_z \tau_{23}) \\ g_{14} &= \hat{\tau}_{13} = J^{-1}(\xi_x \tau_{31} + \xi_y \tau_{32} + \xi_z \tau_{33}) \\ g_{15} &= u\hat{\tau}_{11} + v\hat{\tau}_{12} + w\hat{\tau}_{13} - J^{-1}(\xi_x q_1 + \xi_y q_2 + \xi_z q_3) \end{aligned} \tag{76}$$

$$\hat{G}_2 = \begin{bmatrix} g_{21} \\ g_{22} \\ g_{23} \\ g_{24} \\ g_{25} \end{bmatrix}, \qquad \begin{aligned} g_{21} &= 0 \\ g_{22} &= \hat{\tau}_{21} = J^{-1}(\eta_x \tau_{11} + \eta_y \tau_{12} + \eta_z \tau_{13}) \\ g_{23} &= \hat{\tau}_{22} = J^{-1}(\eta_x \tau_{21} + \eta_y \tau_{22} + \eta_z \tau_{23}) \\ g_{24} &= \hat{\tau}_{23} = J^{-1}(\eta_x \tau_{31} + \eta_y \tau_{32} + \eta_z \tau_{33}) \\ g_{25} &= u\hat{\tau}_{21} + v\hat{\tau}_{22} + w\hat{\tau}_{23} - J^{-1}(\eta_x q_1 + \eta_y q_2 + \eta_z q_3) \end{aligned} \tag{77}$$

$$\hat{G}_3 = \begin{bmatrix} g_{31} \\ g_{32} \\ g_{33} \\ g_{34} \\ g_{35} \end{bmatrix}, \qquad \begin{aligned} g_{31} &= 0 \\ g_{32} &= \hat{\tau}_{31} = J^{-1}(\zeta_x \tau_{11} + \zeta_y \tau_{12} + \zeta_z \tau_{13}) \\ g_{33} &= \hat{\tau}_{32} = J^{-1}(\zeta_x \tau_{21} + \zeta_y \tau_{22} + \zeta_z \tau_{23}) \\ g_{34} &= \hat{\tau}_{33} = J^{-1}(\zeta_x \tau_{31} + \zeta_y \tau_{32} + \zeta_z \tau_{33}) \\ g_{35} &= u\hat{\tau}_{31} + v\hat{\tau}_{32} + w\hat{\tau}_{33} - J^{-1}(\zeta_x q_1 + \zeta_y q_2 + \zeta_z q_3) \end{aligned} \tag{78}$$

$$q_1 = -\alpha \frac{\partial T}{\partial x}, \quad q_2 = -\alpha \frac{\partial T}{\partial y}, \quad q_3 = -\alpha \frac{\partial T}{\partial z}, \qquad \alpha = \frac{1}{(\gamma - 1)R_e}\left(\frac{\mu}{P_r} + \frac{\mu_t}{P_{rt}}\right) \tag{79}$$

From Eqs. (24) and (25), the near-wall shear stress can be written as

$$\tau = \tau_{wall} = \rho_{wall} U_\tau \frac{U_c}{U_c^+} = \frac{\mu_t}{R_e} \frac{U}{y} \tag{80}$$

where μ_t is an effective turbulent viscosity connecting the wall and the first grid point

$$\mu_t = \frac{y^+ \mu_{wall} U_c}{U U_c^+} \tag{81}$$

An advantage of Eq. (80) in calculating separated flows is worthy of note: the direction of the wall shear stress τ_{wall} is determined by that of the flow velocity U while τ_{wall} calculated from Eq. (24) or (2) can only have a positive sign.

From Eq. (80), the general form of shear stress at the first grid point can be expressed as

$$\vec{\tau} = \vec{\tau}_{wall} = \lambda \vec{U}_t \tag{82}$$

where

$$\lambda = \begin{cases} \mu_t/(R_e \Delta n) & \text{if } y^+ > 11.6 \\ \mu_{wall}/(R_e \Delta n) & \text{otherwise} \end{cases} \tag{83}$$

$\vec{U}_t$ and Δn are the tangential component of the resultant velocity and the normal distance from the wall, respectively. Eqs. (82) and (83) simply treat the near-wall region as a

laminar sublayer ($y^+ < 11.6$) and a fully turbulent layer ($y^+ > 11.6$). This treatment prevents the wall function procedure from producing abnormal results when y^+ tends to zero, such as in the vicinity of separation or reattachment points.

Similarly, the total heat flux at the first grid point can be written as

$$q = -\alpha(T - T_{wall}) \tag{84}$$

where

$$\alpha = \begin{cases} \lambda/[(\gamma-1)P_{rt}] & \text{if } y^+ > 11.6 \\ \lambda/[(\gamma-1)P_r] & \text{otherwise} \end{cases} \tag{85}$$

and the heat flux at the wall can be calculated by

$$q_{wall} = -\alpha(T - T_{wall}) - \vec{U}_t \cdot \vec{\tau}_{wall} \tag{86}$$

Consider the wall of η=constant. In this case, only the viscous flux vector $\hat{G}_2$ in Eq. (75) needs to be modified with the use of the wall functions. In the NPARC code, it is calculated by

$$\begin{aligned} \frac{\partial g_{22}}{\partial \eta} &= g_{22,n} - g_{22,s} \\ \frac{\partial g_{23}}{\partial \eta} &= g_{23,n} - g_{23,s} \\ \frac{\partial g_{24}}{\partial \eta} &= g_{24,n} - g_{24,s} \\ \frac{\partial g_{25}}{\partial \eta} &= g_{25,n} - g_{25,s} \end{aligned} \tag{87}$$

where the subscripts s and n refer to the south and north cell faces at j-1/2 and j+1/2. From Eq. (77), the components of the vector $\hat{G}_2$ can be written as

$$\begin{aligned} g_{22} &= J^{-1}(\eta_x^2 + \eta_y^2 + \eta_z^2)\frac{\mu_{tot}}{R_e}\frac{\partial u}{\partial \eta} + \cdots \\ g_{23} &= J^{-1}(\eta_x^2 + \eta_y^2 + \eta_z^2)\frac{\mu_{tot}}{R_e}\frac{\partial v}{\partial \eta} + \cdots \\ g_{24} &= J^{-1}(\eta_x^2 + \eta_y^2 + \eta_z^2)\frac{\mu_{tot}}{R_e}\frac{\partial w}{\partial \eta} + \cdots \\ g_{25} &= u\hat{\tau}_{21} + v\hat{\tau}_{22} + w\hat{\tau}_{23} + J^{-1}(\eta_x^2 + \eta_y^2 + \eta_z^2)\alpha\frac{\partial T}{\partial \eta} + \cdots \end{aligned} \tag{88}$$

with

$$\mu_{tot} = \mu + \mu_t$$

From geometrical consideration, we have

$$J^{-1}(\eta_x^2+\eta_y^2+\eta_z^2)=\frac{J^{-2}(\eta_x^2+\eta_y^2+\eta_z^2)}{J^{-1}}=\frac{\Delta S^2}{\Delta\Omega}=\frac{\Delta S}{\Delta n}\quad(\Delta\Omega=\Delta S\Delta n) \tag{89}$$

where $\Delta\Omega$ and ΔS are the volume and face area of the control volume, respectively.

In the wall function approach, all the stresses acting on the cell face considered are replaced by the wall shear stress given by Eq. (82). Therefore, for the south wall, Eqs. (88) are replaced by

$$\begin{aligned}
g_{22,s}&=\Delta S\frac{\mu_{tot}}{R_e\Delta n}u_{t,x}=\Delta S\lambda u_{t,x}\\
g_{23,s}&=\Delta S\frac{\mu_{tot}}{R_e\Delta n}u_{t,y}=\Delta S\lambda u_{t,y}\\
g_{24,s}&=\Delta S\frac{\mu_{tot}}{R_e\Delta n}u_{t,z}=\Delta S\lambda u_{t,z}\\
g_{25,s}&=ug_{22,s}+vg_{23,s}+wg_{24,s}+\Delta S\alpha(T-T_{wall})
\end{aligned} \tag{90}$$

where $u_{t,x}$, $u_{t,y}$, $u_{t,z}$ are the x-, y-, z-component of the tangential velocity $\vec{U}_t$, respectively. If n_x, n_y and n_z are the Cartesian components of the unit normal vector at the wall, $u_{t,x}$, $u_{t,y}$, $u_{t,z}$ can be calculated by

$$\begin{aligned}
u_{t,x}&=u-n_xV_n\\
u_{t,y}&=v-n_yV_n\\
u_{t,z}&=w-n_zV_n
\end{aligned} \tag{91}$$

with

$$V_n=n_xu+n_yv+n_zw$$

Similarly, for the north wall, we have

$$\begin{aligned}
g_{22,n}&=-\Delta S\frac{\mu_{tot}}{R_e\Delta n}u_{t,x}=-\Delta S\lambda u_{t,x}\\
g_{23,n}&=-\Delta S\frac{\mu_{tot}}{R_e\Delta n}u_{t,y}=-\Delta S\lambda u_{t,y}\\
g_{24,n}&=-\Delta S\frac{\mu_{tot}}{R_e\Delta n}u_{t,z}=-\Delta S\lambda u_{t,z}\\
g_{25,n}&=ug_{22,n}+vg_{23,n}+wg_{24,n}-\Delta S\alpha(T-T_{wall})
\end{aligned} \tag{92}$$

Walls in the other two directions can be treated in the same way.

The sequence in which the above equations are solved together with the Navier-Stokes and turbulence equations in the code is as follows:

a. Initialize all field values.

b. Calculate τ_{wall} and y^+ using Eqs. (82) and (25).

c. Fix the values of K and ϵ at the first grid points using Eqs. (29) and (30).

d. Solve the turbulence equations.

e. Calculate q_{wall} using Eq. (86).

f. Calculate U_c and U_c^+ using Eqs. (26) and (24).

g. Update μ_t using Eq. (81).

h. Update α using Eq. (85).

i. Update g_{22}, g_{23}, g_{24} and g_{25} using Eq. (90) or (92).

j. Solve the Navier-Stokes equations.

k. Return to step b with updated field values.

The sequence of steps b to k are repeated until the calculation converges.

Note that by definition, the turbulent eddy-viscosity μ_t is zero at the wall, such as in the case of the low Reynolds number turbulence models. When using the wall functions, Eq. (81) introduces the effective turbulent viscosity which is defined at the wall in the turbulence module. Therefore in post-processing, the wall friction coefficient C_f can be calculated in the same way as for laminar flows, except that the molecular viscosity μ is replaced by the turbulent viscosity μ_t at the wall.

4 Module Usage

The present turbulence module (version 2.0) is written based on the NPARC version 2.2. The following are those parts of the code which may require user's attention when using it.

4.1 Module

To facilitate identification, all the subroutine names in the module start with CM. In order to use the module, the user only needs to call its three subroutines: CMA0, CMALL and CMVRHS, in the NPARC code.

• **Subroutine CMA0.** This subroutine transfers from NPARC to the module the parameters to define flow, geometric and boundary conditions. In addition, it has the following user-specified parameters:

JWFAV, KWFAV, LWFAV — Number of grid points above J-, K-, and L-walls at which the artificial viscosity is turned off when using the wall function approach. These numbers should cover the near-wall region within $y^+ \approx 1000$. Currently, they are set to

JWFAV=5, KWFAV=5, LWFAV=5

FDEFER — Blending factor in the convection scheme. Its value may vary from 0 to 1 with the limiting value 0 for the first-order accurate upwind and 1 for the second-order accurate HLPA scheme. The solution tends to be more stable, but also more diffusive when this factor is reduced.

BDMAX(i), BDMIN(i) — Upper and lower bounds for the values of K (i=1), ϵ (i=2) and μ_t (i=3). These bounds are introduced for numerical purposes only, that is, to prevent the corresponding turbulence quantities from becoming negative or abnormally large during the solution process. Currently, they are set to

BDMAX(1)=1.0E+6, BDMIN(1)=1.0E-8
BDMAX(2)=1.0E+6, BDMIN(2)=1.0E-8
BDMAX(3)=1.0E+4, BDMIN(3)=1.0E-3

which should cover a wide range of the physically meaningful values of K, ϵ and μ_t. It is to be noted that these values are only valid for the non-dimensional turbulence quantities, as defined in the NPARC code.

• **Subroutine CMALL.** This is the main subroutine to control the solution sequence in the module. The array variable VIST is the turbulent viscosity μ_t which is needed in NPARC for calculating turbulent flows. The array variables TE, ED and YPS are K, ϵ and y^+, respectively, which can be used for post-processing. Normally, there is no need for user to change this subroutine.

• **Subroutine CMVRHS.** This subroutine which is the counterpart of the subroutine

VISRHS in NPARC is for introducing the wall function modifications into the right-hand side viscous flux terms. There is no need for user to change this subroutine.

4.2 NPARC

The authors have made all the modifications necessary for NPARC to use the module. The following shows where these modifications are in NPARC. All the alterations are marked between C<< and C>> in the code.

• **Namelist TURBIN.** The integer parameter IMUTR2 is used to select the turbulence models in the module with

IMUTR2=101 Chien model
102 Shih-Lumley model
103 CMOTT model

A new integer parameter MWALF is introduced to select the near-wall approach with

MWALF=0 low Reynolds number approach
1 wall function approach

Correspondingly, a new statement is added
in the include file NPARC.INC:
COMMON/CMOTT/MWALF
and in the subroutine TURBIN:
CALL NLGETI('MWALF',MWALF).

• **Subroutines FILT1, FILT2, FILTER.** An array FAV01 has been introduced into each of these subroutines to eliminate the artificial viscosity in the near-wall region when using the wall function approach.

• **Subroutine DEPOIN.** For using the module, an additional array whose name is IPWCM1 is added to IPWLST, and MEMSIZ in NPARC.INC must be increased correspondingly.

• **Subroutines INITIA, WREST.** The model identifier ITURB for each K-ϵ turbulence model in the module is given an integer value greater than 100. To reflect this expanded choice for turbulence models, the read and write statements for the turbulent quantities in these two subroutines are modified as

```
IF(ITURB.EQ.4 .OR.
&  ITURB.EQ.5 .OR.
&  ITURB.EQ.7 .OR.
&  ITURB.GT.100)
&  READ(2) or WRITE(4) (values of K, ε, μt)
```

• **Subroutine MUTURB.** Here, the subroutines CMA0 and CMALL of the module are called as follows:

```
        ......
        ELSE IF(ITURB.EQ.7) THEN
        CALL TKWSTEP(BIGA(IPWR),BIGA(IPWAK),BIGA(IPWEPS)
      &,BIGA(IPWS1))
C<<
        ELSE IF(ITURB.EQ.101 .OR. ITURB.EQ.102 .OR. ITURB.EQ.103) THEN
        CALL CMA0(JMAX,KMAX,LMAX,NMAX,NTURB,NRLX,NSPRT,ITURB
      &,MWALF
      &,RE,C2B,GAMMA,RPR,RPRT,DT,DTCAP,IVARDT
      &,TUIN1,TUIN2,TUIN3,TMUIN1,TMUIN2,TMUIN3
      &,NJPAT,JPJ2,JPJM,JPK2,JPKM,JPL2,JPLM
      &,NKPAT,KPJ2,KPJM,KPK2,KPKM,KPL2,KPLM
      &,NLPAT,LPJ2,LPJM,LPK2,LPKM,LPL2,LPLM
      &,NJSEG,JLINE,JKLOW,JKHIGH,JLLOW,JLHIGH,JTYPE,JSIGN,JEDGE
      &,TEMPJ
      &,NKSEG,KLINE,KJLOW,KJHIGH,KLLOW,KLHIGH,KTYPE,KSIGN,KEDGE
      &,TEMPK
      &,NLSEG,LLINE,LJLOW,LJHIGH,LKLOW,LKHIGH,LTYPE,LSIGN,LEDGE
      &,TEMPL)
C
        IPWR3=IPWS1+2*NXYZ
        IPWR4=IPWR3+NXYZ
        CALL CMALL(BIGA(IPWX ),BIGA(IPWY ),BIGA(IPWZ )
      &,BIGA(IPWXX ),BIGA(IPWXY ),BIGA(IPWXZ )
      &,BIGA(IPWYX ),BIGA(IPWYY ),BIGA(IPWYZ )
      &,BIGA(IPWZX ),BIGA(IPWZY ),BIGA(IPWZZ ),BIGA(IPWQ )
      &,BIGA(IPWR ),BIGA(IPWRU ),BIGA(IPWRV ),BIGA(IPWRW )
      &,BIGA(IPWE ),BIGA(IPWAK ),BIGA(IPWEPS),BIGA(IPWTMU)
      &,BIGA(IPWR3 ),BIGA(IPW28 ),BIGA(IPW29 ),BIGA(IPWR4 )
      &,BIGA(IPWVDT),BIGA(IPWS1 )
      &,BIGA(IPWS1 + 4*NXYZ ),BIGA(IPWSPT),BIGA(IPWCOF)
      &,NC,SUMN,TMAX)
C>>
        ELSE
        ......
        END IF
```

• **Subroutine STPF3D.** The subroutine CMVRHS of the module is called here.

5 Demonstration Examples

Two examples are given here to demenstrate how to use the NPARC code with the turbulence module. Other application examples can be found in Yang et al. (1995).

5.1 Flat Plate

Turbulent boundary layer flow over a flat plate with zero pressure gradient was selected as the first test case for code validation. The solutions of both the low Reynolds number (LR) and the wall function (WF) approaches were compared with the experimental data (Exp) of Wieghardt and Tillmann (1951). Fig.1 shows the flow geometry and boundary conditions used in the calculation. For the wall function approach, grid points were 111×55×5, the first grid points above the wall had the y^+ value of 60 and 14 grid points in the x-direction were located before the leading edge of the flat plate. For the low Reynolds number approach, grid points were 111×81×5 with the distribution of x-points being the same as in the wall function case and the first y^+ being 0.3. Since the NPARC code is for compressible flows while the experiment to be compared was for incompressible flows, a freestream Mach number of 0.2 was chosen. All calculations started from an initial field with $U = 0.2, V = 0, \mu_t = 1, K = 0.005$ and $\epsilon = 0.09 R_e K^2/\mu_t$. The detailed NPARC input data are given in Appendix 2. Fig.2 shows the convergence history of the Chien model. The other two models had the similar convergence behavior. For comparison, the result of the Baldwin-Lomax model in the NPARC code is also given in Fig.2. The low Reynolds number Chien model had a rather poor convergence behavior: its L2 norm of residual was only reduced to 4.7×10^{-8} after 20000 iterations, and further down to 8.9×10^{-10} after another 60000 iterations. However, the solutions at both the 20000th and 80000th iterations were almost identical. Fig.3 shows the wall friction coefficient C_f versus the Reynolds number based on the momentum thickness of boundary layer Re_θ. It can be seen that for the the low Reynolds number approach, the results of both the Shih-Lumley and CMOTT models are almost the same and slightly better than that of the Chien model, while for the wall function approach, the results of both the Chien and Shih-Lumley models are almost identical and slightly better than that of the CMOTT model. Regarding the computational cost of the Chien model, 1000 iterations on the Cray YMP computer took 1566 seconds for the wall function approach and 2320 seconds for the low Reynolds number approach.

5.2 Transonic Diffuser

This case was taken from the experiment of Salmon et al. (1983). Fig.4 shows the computational domain of the diffuser. In the experiment, different measurements were taken, ranging from no-shock to strong-shock conditions. During the code validation, we calculated three cases with no-shock, weak-shock and strong-shock, respectively. Here, we only show the strong-shock case which is most difficult to calculate accurately. All calculations started from an initial field with $U = 0.44, V = 0, p = 0.5143, \mu_t = 10, K =$

0.0001 and $\epsilon = 0.09 R_e K^2/\mu_t$. For the low Reynolds number approach, the grid had 81×81×5 points and its x-point distribution was the same as that used by Dudek (1995), and for the wall function approach, the grid had 81×51×5, differing from the former one only in the y direction. The detailed NPARC input data are given in Appendix 2. Fig.5 shows the convergence history, and it can be seen that the wall function approach has a better convergence behavior than the low Reynolds number approach. The pressure distributions are shown in Fig.6 for the top wall and in Fig.7 for the bottom wall. For the low Reynolds number approach, the CMOTT model gave the best results, especially for the location of the shock wave and the pressure recovery after the shock wave, while for the wall function approach, the results of the CMOTT model were slightly worse than those of the other two K-ϵ model. Fig.8 shows the streamwise mean velocity profile at the section x/X_{ref}=4.6, and it can be seen that the results of all the three K-ϵ models with the wall functions are nearly the same, and better than those of the low Reynolds number counterpart. For the computational cost of the Chien model, 1000 iterations took 1088 seconds for the wall function approach and 1720 seconds for the low Reynolds number approach.

References

[1] Chien, K.Y., "Predictions of channel and boundary-layer flows with a low Reynolds number turbulence model," *AIAA Journal*, Vol.20, 1982, pp.33-38.

[2] Chitsomboon, T., "Effects of artificial viscosity on the accuracy of high Reynolds number K-ϵ turbulence model," NASA TM 106781, 1994.

[3] Cooper, G.K., and Sirbaugh, J.R., "PARC code: theory and usage," AEDC-TR-89-15, Arnold Engineering Development Center, 1989.

[4] Cooper, G.K., and Sirbaugh, J.R., "The PARC distinction: a practical flow simulator," AIAA 90-2002, 1990.

[5] Dudek, J.C., "NPARC example case - Transonic diffuser flow," NASA Lewis Research Center, 1995.

[6] Gaskell, P.H., and Lau, A.K.C., "Curvature-compensated convective transport: SMART, A new boundedness preserving transport algorithm," *International Journal for Numerical Methods in Fluids*, Vol.8, 1988, pp.617-641.

[7] Huang, P.G., and Coakley, T.J., "Calculations of supersonic and hypersonic flows using compressible wall functions," presented at the 2nd Int. Symp. on Turbulence Modeling and Measurement, 1993, Florence, Italy.

[8] Launder, B.E., and Spalding, D.B., "The numerical computation of turbulent flows," *Computer Methods in Applied Mechanics and Engineering*, Vol.3, 1974, pp.269-289.

[9] Leonard, B.P., "Simple high-accuracy resolution program for convective modeling of discontinuities," *Int. J. for Num. Methods in Fluids*, Vol.8, 1988, pp.1291-1318.

[10] Patel, V.C., Rodi, W. and Scheuerer, G., "Turbulence models for near wall and low Reynolds number flows: a review," *AIAA Journal*, Vol.23, 1985, pp.1308-1319.

[11] Salmon, J.T., Bogar, T.J., and Sajben, M., "Laser Doppler velocimeter measurements in unsteady, separated, transonic diffuser flows," *AIAA Journal*, Vol.21, 1983, pp.1690-1697.

[12] Shih, T.-H., and Lumley, J.L., "Kolmogorov behavior of near-wall turbulence and its application in turbulence modeling," *Comp. Fluid Dyn.*, Vol.1, 1993, pp.43-56.

[13] Shih, T.-H., Zhu, J. and Lumley, J.L., "A new Reynolds stress algebraic equation model," NASA TM 106644, 1994, also in *Computer Methods in Applied Mechanics and Engineering*, Vol.125, 1995, pp.287-302.

[14] Shih, T.-H., Liou, W.W., Shabbir, A., Yang, Z. and Zhu, J., "A new K-ϵ eddy viscosity model for high Reynolds number turbulent flows - Model development and validation," *Computers and Fluids*, Vol.24, No.3, 1995, pp.227-238.

[15] Van Driest, E.R., "Turbulent boundary layer in compression fluids," *J. Aeronaut. Sci.*, Vol.18, 1951, pp.145-160.

[16] Viegas, J.R., Rubesin, M.W., and Horstman, C.C., "On the use of wall functions as boundary conditions for two dimensional separated compressible flows," AIAA 85-0180, 1985.

[17] Wieghardt, K., and Tillmann, W., "On the turbulent friction layer for rising pressure," NACA TM 1314, 1951.

[18] Yang, Z., Georgiadis, N.J., Zhu, J. and Shih, T.-H., "Calculations of inlet/nozzle flows using a new K-ϵ model," AIAA 95-2761, 1995.

[19] Zhu, J., "A low diffusive and oscillation-free convection scheme," *Communications in Applied Numerical Methods.*, Vol.7, 1991, pp.225-232.

[20] Zhu, J., "On the higher-order bounded discretization schemes for finite-volume computations of incompressible flows ," *Computer Methods in Applied Mechanics and Engineering*, Vol.98, 1992, pp.345-360.

[21] Zhu, J., and Shih, T.-H., "A turbulence module for the NPARC code," AIAA 95-2612, 1995.

APPENDIX 1: Figures

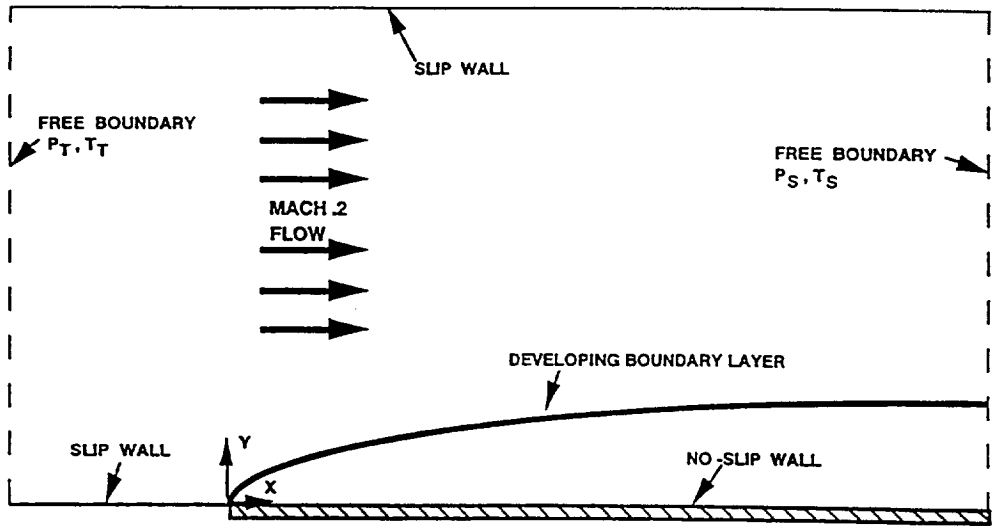

Fig.1 Flow geometry and boundary conditions

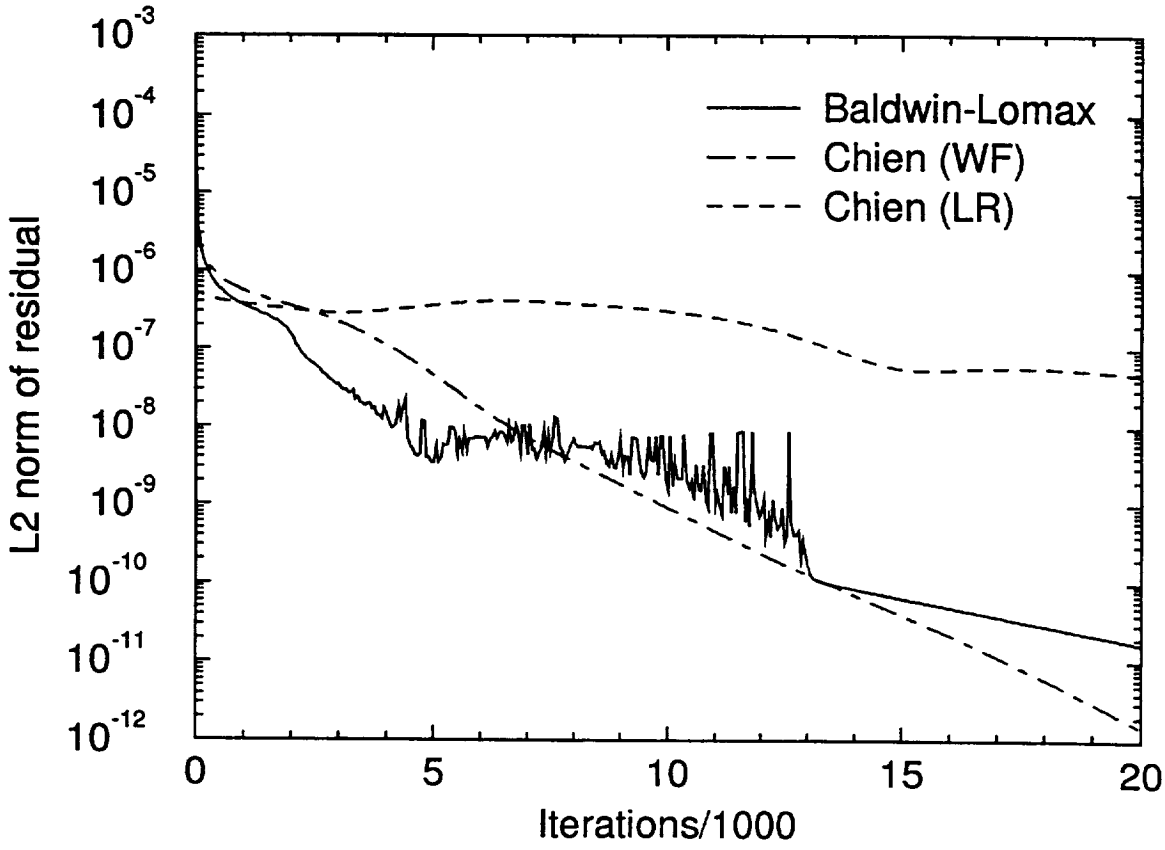

Fig.2 Convergence history

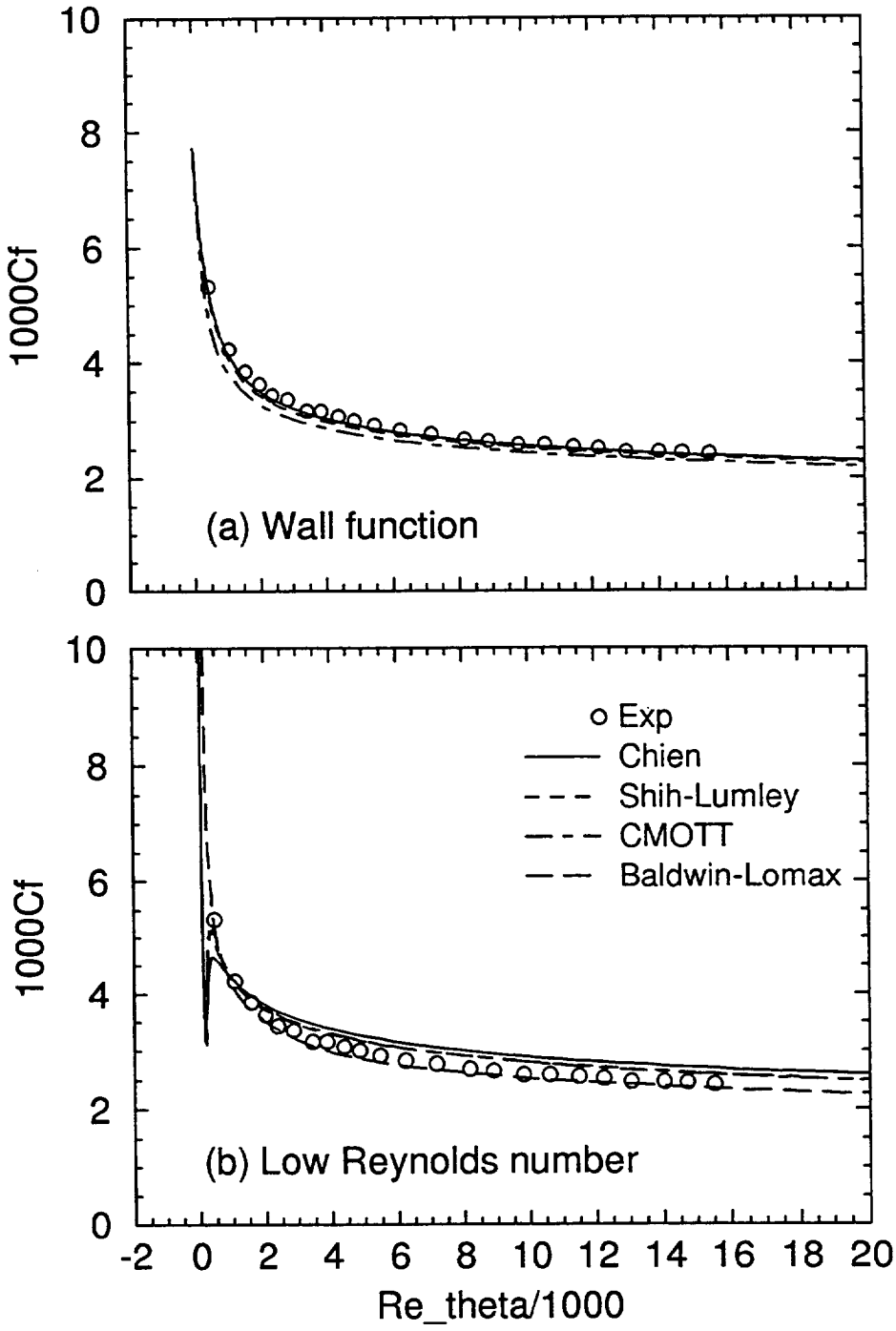

Fig.3 Wall friction coefficient

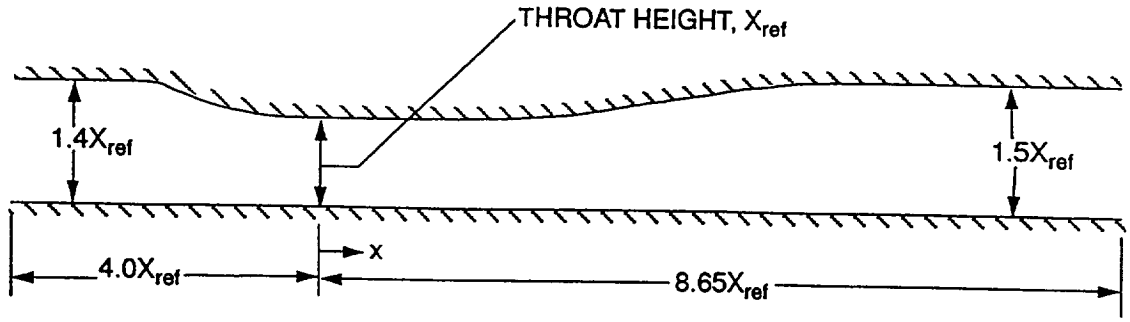

Fig.4 Computational domain of diffuser

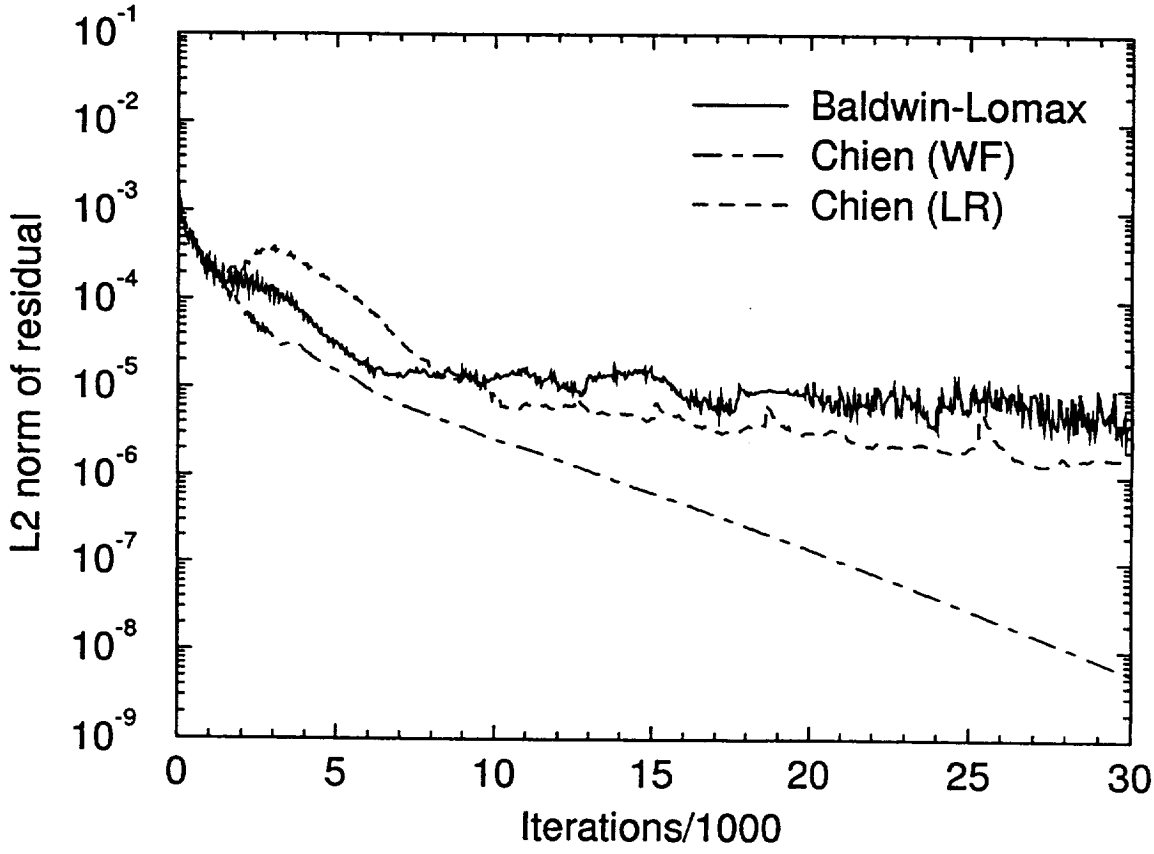

Fig.5 Convergence history

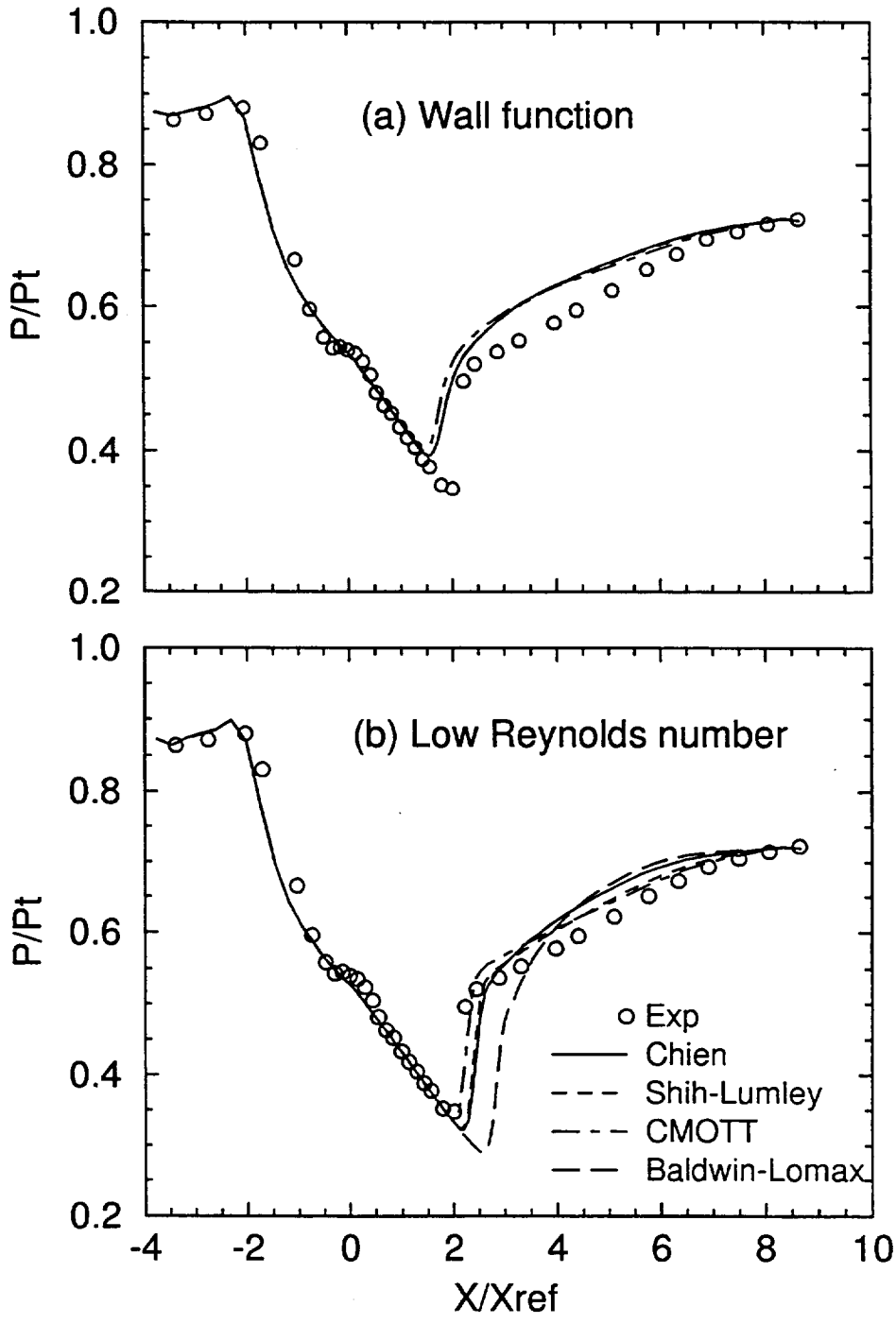

Fig.6 Pressure distribution at the top wall

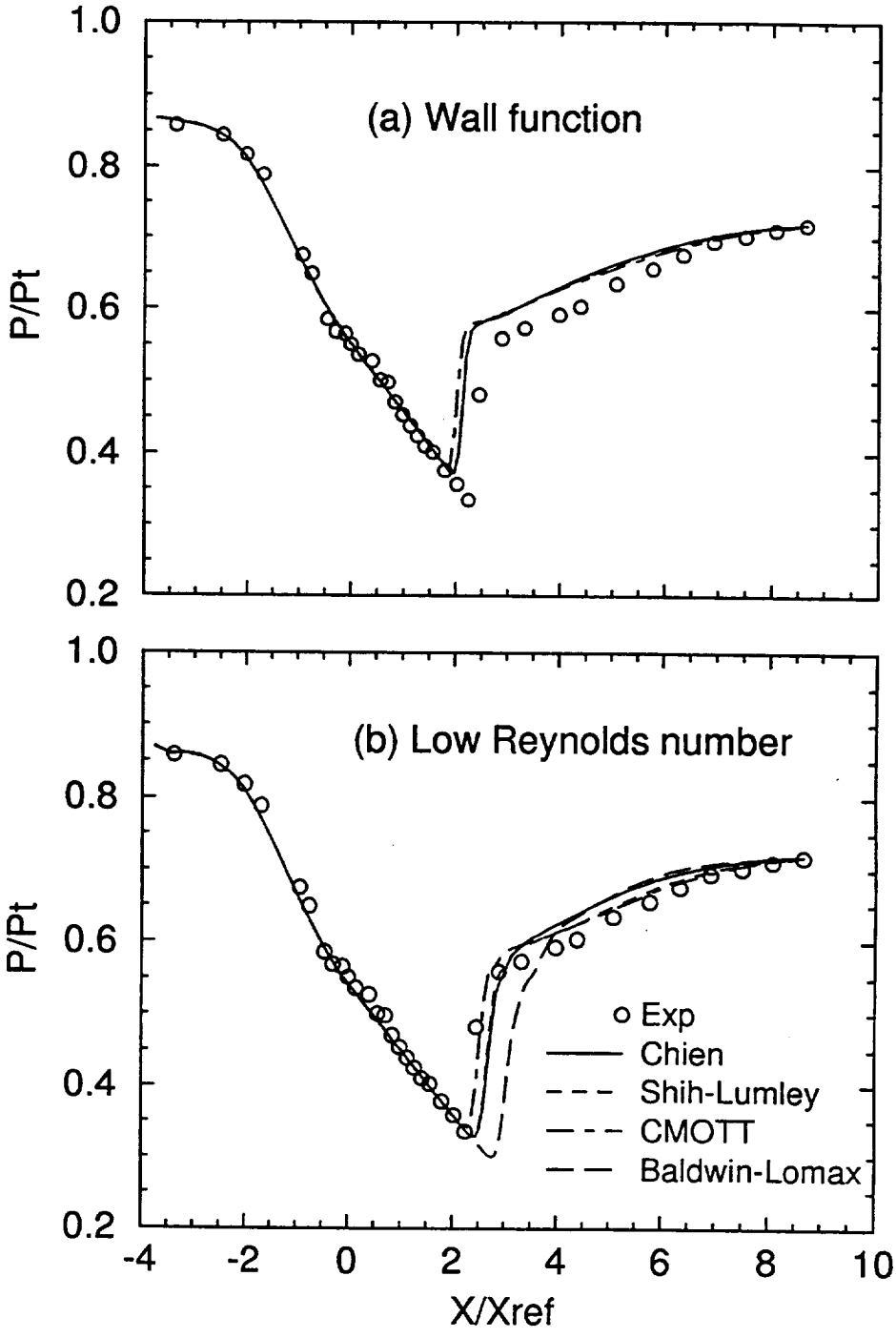

Fig.7 Pressure distribution at the bottom wall

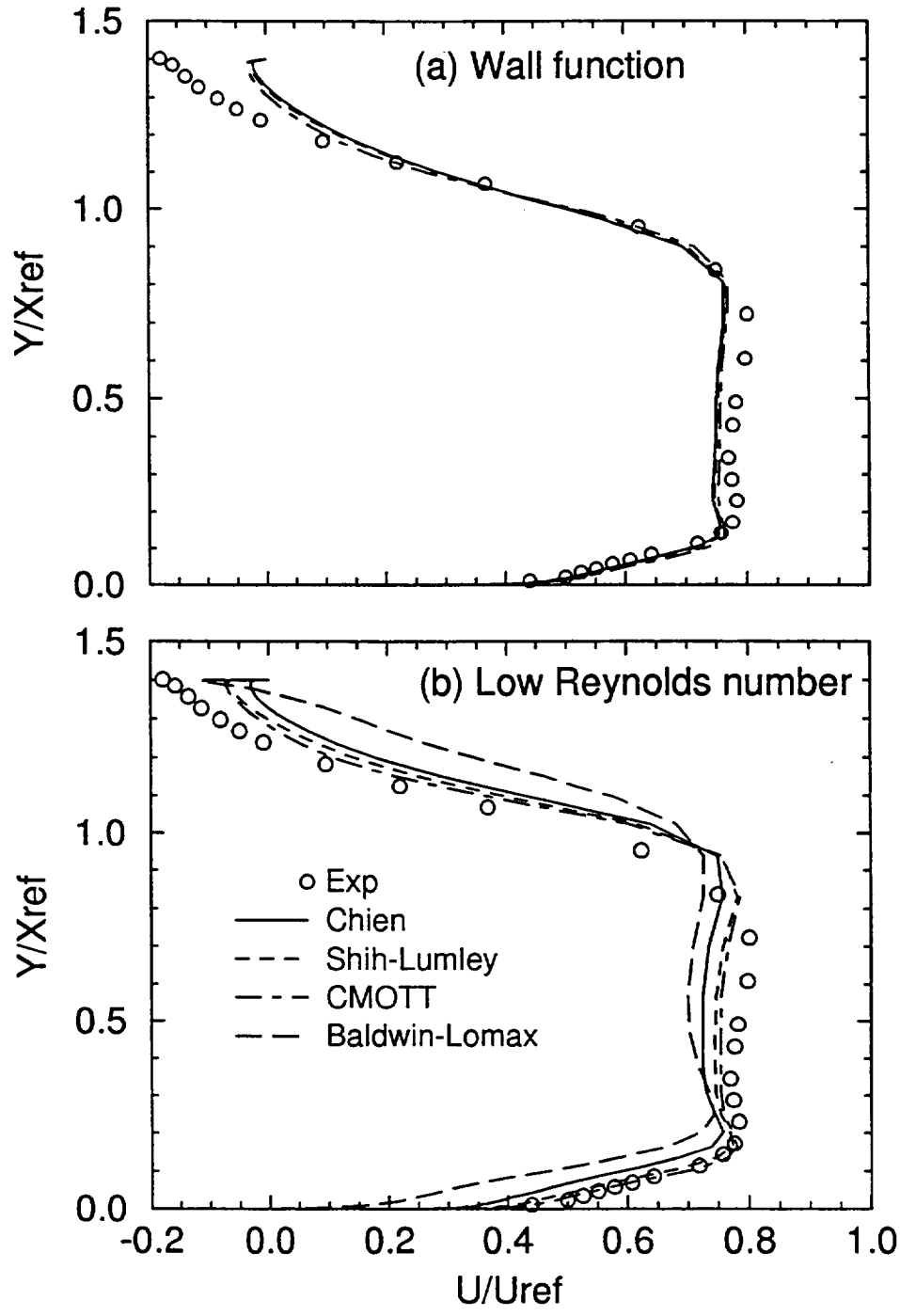

Fig.8 Streamwise mean velocity profile at x/X_{ref}=4.6

7 APPENDIX 2: NPARC Input Files

- **Flat Plate Case, Wall Function Approach**

```
$INPUTS
    pref    =   2116.80        ,      nblock  =     1 ,
    trefr   =   519.0          ,      nmax    =  1000 ,
    vrat    =   1.000001e+00   ,      nc      =    -1 ,
    tsuth   =   0.198680e+03   ,      nsprt   =    50 ,
    re      =   5.000000e+06   ,      np      = 960000,
    pr      =   0.720000e+00   ,      ifxprt  =     0 ,
                                       ifxplt  =     0 ,
    dtcap   =   5.0            ,      l2plot  =    -1 ,
    pcqmax  =   1.000000e+01   ,      iplot   =     0 ,
    splend  =   0.500000e+00   ,
    stopl2  =   1.000000e-15   ,      numdt   =     0 ,
    stoptr  =   100.0          ,      ivardt  =     2 ,
    xmach   =   0.200000e+00   ,      ifiltr  =     2 ,
                                       ispect  =     1 ,
    gamma   =   1.400000e+00   ,      lrest   =     1 ,
    dis2    =   0.250000e+00   ,      mbord   =     1 ,
    dis4    =   0.640000E+00   ,      ibord   =     1 ,
$END
$TURBIN
    imutur  =  101,
    imutr2  =  101,
    mwalf   =    1,
    nturb   =    0,
    order   =  1.0,
    nrlx    =    1,
    ifmax   =    3,
    prt     =  0.9,
    tuin1   = 0.02,
    tmuin1  = 10.0,
$END
$BLOCK
     invisc(1) = 1,     invisc(2) = 1,     invisc(3) = 1,
     lamin(1)  = 0,     lamin(2)  = 1,     lamin(3)  = 0,
     npseg     = 1,     nbcseg    = 7,
$END
$PRTSEG
     jklpi(1,1,1) =   1,  55,  55,
     jklpi(1,2,1) =   1,  55,  10,
     jklpi(1,3,1) =   3,   3,   1,
     ipord(1,1)   =   2,   1,   3,
$END
   1    1    2   54    1    5    0    1          0.7345000 1.0080000   -1
 111  111    2   54    1    5    0   -1          0.7143000 1.0000000    0
   1   14    1    1    1    5   50    1
  15  111    1    1    1    5   60    1                                 50
   1  111   55   55    1    5   50   -1
   1  111    1   55    1    1   50    1
   1  111    1   55    5    5   50   -1
```

- **Flat Plate Case, Low Reynolds Number Approach**

```
$INPUTS
    pref    =   2116.80        ,      nblock  =     1 ,
    trefr   =   519.0          ,      nmax    =  1000 ,
    vrat    =   1.000001e+00   ,      nc      =    -1 ,
    tsuth   =   0.198680e+03   ,      nsprt   =    50 ,
    re      =   5.000000e+06   ,      np      = 960000,
    pr      =   0.720000e+00   ,      ifxprt  =     0 ,
                                       ifxplt  =     0 ,
    dtcap   =   1.0            ,      l2plot  =    -1 ,
    pcqmax  =   1.000000e+01   ,      iplot   =     0 ,
    splend  =   0.500000e+00   ,
    stopl2  =   1.000000e-15   ,      numdt   =     0 ,
    stoptr  =   100.0          ,      ivardt  =     2 ,
    xmach   =   0.200000e+00   ,      ifiltr  =     2 ,
                                       ispect  =     1 ,
    gamma   =   1.400000e+00   ,      lrest   =     1 ,
    dis2    =   0.250000e+00   ,      mbord   =     1 ,
    dis4    =   0.640000E+00   ,      ibord   =     1 ,
$END
$TURBIN
    imutur  =    2,
    imutr2  =  101,
    mwalf   =    0,
    nturb   = 4001,
    order   =  1.0,
    nrlx    =  100,
    ifmax   =    3,
    prt     =  0.9,
    tuin1   = 0.02,
    tmuin1  = 10.0,
$END
$BLOCK
     invisc(1) = 1,     invisc(2) = 1,     invisc(3) = 1,
     lamin(1)  = 0,     lamin(2)  = 1,     lamin(3)  = 0,
     npseg     = 1,     nbcseg    = 7,
$END
$PRTSEG
     jklpi(1,1,1) =   1,  81,  81,
     jklpi(1,2,1) =   1,  81,  10,
     jklpi(1,3,1) =   3,   3,   1,
     ipord(1,1)   =   2,   1,   3,
$END
   1    1    2   80    1    5    0    1          0.7345000 1.0080000   -1
 111  111    2   80    1    5    0   -1          0.7143000 1.0000000    0
   1   14    1    1    1    5   50    1
  15  111    1    1    1    5   60    1                                  70
   1  111   81   81    1    5   50   -1
   1  111    1   81    1    1   50    1
   1  111    1   81    5    5   50   -1
```

- **Transonic Diffuser Case, Wall Function Approach**

```
$INPUTS
    pref    =   2819.5          ,       nblock  =      1 ,
    trefr   =   525.6           ,       nmax    =   1000 ,
    vrat    =   0.100000e+01    ,       nc      =     -1 ,
    tsuth   =   0.198680e+03    ,       nsprt   =     50 ,
    re      =   1.339171e+06    ,       np      = 900000 ,
    pr      =   0.720000e+00    ,       ifxprt  =      0 ,
                                        ifxplt  =      0 ,
    dtcap   =   0.5             ,       l2plot  =     -1 ,
    pcqmax  =   10.0            ,       iplot   =      0 ,
    splend  =   0.50            ,
    stopl2  =   1.000000e-15    ,       numdt   =      0 ,
    stoptr  =   100.0           ,       ivardt  =      2 ,
    xmach   =   0.10            ,       ifiltr  =      2 ,
                                        ispect  =      1 ,
    gamma   =   1.40            ,       lrest   =      1 ,
    dis2    =   0.25            ,       ibord   =      1 ,
    dis4    =   0.64            ,       mbord   =      1 ,
$END
$TURBIN
    imutur  =    2,
    imutr2  =  101,
    mwalf   =    1,
    nturb   =    0,
    order   =  1.0,
    nrlx    =    1,
    ifmax   =    2,
    prt     =  0.9,
    tuinl   = 0.02,
    tmuinl  = 10.0,
$END
$BLOCK
     invisc(1)=1, invisc(2)=1, invisc(3)=1,
     lamin(1) =1, lamin(2) =1, lamin(3) =1,
     npseg    =1, nbcseg   =6,
$END
$PRTSEG
     jklpi(1,1,1) =   1,  41,  41,
     jklpi(1,2,1) =   1,  51,  10,
     jklpi(1,3,1) =   3,   3,   1,
     ipord(1,1)   =   2,   1,   3,
$END
   1    1    2   50    1    5    0    1          0.7143000 1.0000000   -1
  81   81    2   50    1    5    0   -1          0.5143000 0.5000000    0
   1   81    1    1    1    5   60    1                                 25
   1   81   51   51    1    5   60   -1                                 25
   1   81    1   51    1    1   50    1
   1   81    1   51    5    5   50   -1
```

- **Transonic Diffuser Case, Low Reynolds Number Approach**

```
$INPUTS
    pref    =   2819.5          ,       nblock  =      1 ,
    trefr   =   525.6           ,       nmax    =   1000 ,
    vrat    =   0.100000e+01    ,       nc      =     -1 ,
    tsuth   =   0.198680e+03    ,       nsprt   =     50 ,
    re      =   1.339171e+06    ,       np      = 900000 ,
    pr      =   0.720000e+00    ,       ifxprt  =      0 ,
                                        ifxplt  =      0 ,
    dtcap   =   0.5             ,       l2plot  =     -1 ,
    pcqmax  =   10.0            ,       iplot   =      0 ,
    splend  =   0.50            ,
    stopl2  =   1.000000e-15    ,       numdt   =      0 ,
    stoptr  =   100.0           ,       ivardt  =      2 ,
    xmach   =   0.10            ,       ifiltr  =      2 ,
                                        ispect  =      1 ,
    gamma   =   1.40            ,       lrest   =      1 ,
    dis2    =   0.25            ,       ibord   =      1 ,
    dis4    =   0.64            ,       mbord   =      1 ,
$END
$TURBIN
    imutur  =    2,
    imutr2  =  101,
    mwalf   =    0,
    nturb   =    0,
    order   =  1.0,
    nrlx    =    1,
    ifmax   =    2,
    prt     =  0.9,
    tuin1   = 0.02,
    tmuin1  = 10.0,
$END
$BLOCK
     invisc(1)=1, invisc(2)=1, invisc(3)=1,
     lamin(1) =1, lamin(2) =1, lamin(3) =1,
     npseg    =1, nbcseg   =6,
$END
$PRTSEG
     jklpi(1,1,1) =   1,  41,  41,
     jklpi(1,2,1) =   1,  81,  10,
     jklpi(1,3,1) =   3,   3,   1,
     ipord(1,1)   =   2,   1,   3,
$END
   1    1    2   80    1    5    0    1          0.7143000 1.0000000   -1
  81   81    2   80    1    5    0   -1          0.5143000 0.5000000    0
   1   81    1    1    1    5   60    1                                 40
   1   81   81   81    1    5   60   -1                                 41
   1   81    1   81    1    1   50    1
   1   81    1   81    5    5   50   -1
```

REPORT DOCUMENTATION PAGE

Form Approved
OMB No. 0704-0188

1. AGENCY USE ONLY (*Leave blank*)	2. REPORT DATE	3. REPORT TYPE AND DATES COVERED
	August 1997	Contractor Report

4. TITLE AND SUBTITLE

CMOTT Turbulence Module for NPARC

5. FUNDING NUMBERS

WU–522–31–23–00
NCC3–520

6. AUTHOR(S)

J. Zhu and T.-H. Shih

7. PERFORMING ORGANIZATION NAME(S) AND ADDRESS(ES)

Institute for Computational Mechanics in Propulsion
22800 Cedar Point Road
Cleveland, Ohio 44142

8. PERFORMING ORGANIZATION REPORT NUMBER

E–10878

9. SPONSORING/MONITORING AGENCY NAME(S) AND ADDRESS(ES)

National Aeronautics and Space Administration
Lewis Research Center
Cleveland, Ohio 44135–3191

10. SPONSORING/MONITORING AGENCY REPORT NUMBER

NASA CR–204143
ICOMP–97–10; CMOTT–97–05

11. SUPPLEMENTARY NOTES

ICOMP Program Director, Louis A. Povinelli, organization code 5800, (216) 433–5818.

12a. DISTRIBUTION/AVAILABILITY STATEMENT

Unclassified - Unlimited
Subject Category 34

This publication is available from the NASA Center for AeroSpace Information, (301) 621–0390.

12b. DISTRIBUTION CODE

13. ABSTRACT ***(Maximum 200 words)***

This is a user's manual of the CMOTT turbulence module, version 2.0, developed for the NPARC code. The module is written in a self-contained manner so that the user can use any turbulence model in the module without concern as to how it is implemented and solved. Three two-equation turbulence models have been built into the module: Chien, Shih-Lumley and CMOTT models, and all of them have both the low Reynolds number and wall function options. Unlike Chien's model, both the Shih-Lumley and CMOTT models do not involve the dimensionless wall distance y^+ in the low Reynolds number approach, an advantage for separated flow calculations. The Van Driest transformation is used so that the wall functions can be applied to both incompressible and compressible flows. The manual gives the details of the turbulence models used and their numerical implementation. It also gives two application examples, one for subsonic and the other for transonic flow, for demonstration. The module can be easily linked to the NPARC code for practical applications.

14. SUBJECT TERMS

Turbulence modeling; Wall function; Computer code; Navier-Stokes solver

15. NUMBER OF PAGES

37

16. PRICE CODE

A03

17. SECURITY CLASSIFICATION OF REPORT	18. SECURITY CLASSIFICATION OF THIS PAGE	19. SECURITY CLASSIFICATION OF ABSTRACT	20. LIMITATION OF ABSTRACT
Unclassified	Unclassified	Unclassified	